



## A study about evolutionary and non-evolutionary segmentation techniques on hand radiographs for bone age assessment

Shreyas Simu, Shyam Lal\*

Department of Electronics & Communication Engineering, National Institute of Technology Karnataka, Surathkal, Mangaluru - 575025, India



### ARTICLE INFO

#### Article history:

Received 4 June 2016

Received in revised form 22 October 2016

Accepted 16 November 2016

#### Keywords:

Hand bone segmentation

Bone age assessment

Evolutionary algorithms

Non-evolutionary algorithms

### ABSTRACT

In this paper, a study and performance comparison of various evolutionary and non-evolutionary segmentation techniques on digital hand radiographs for bone age assessment is presented. The segmented hand bones are of vital importance in process of automated bone age assessment (ABAA). Bone age assessment is a technique of checking the skeletal development and detecting growth disorder in a person. However, it is very difficult to segment out the bone from the soft tissue. The problem arises from overlapping pixel intensities between bone region and soft tissue region and also between soft tissue region and background. Thus there is a requirement for a robust segmentation technique for hand bone segmentation. Taking this into consideration we make a comparison between non-evolutionary and evolutionary segmentation algorithms implemented on hand radiographs to recognize bone borders and shapes. The simulation and experimental results demonstrate that multiplicative intrinsic component optimization (MICO) algorithm provides better results as compared to other existing evolutionary and non-evolutionary algorithms.

© 2016 Elsevier Ltd. All rights reserved.

### 1. Introduction

Bone age assessment (BAA) is one of the most important procedures for the evaluation of biological maturity of children whose age is unknown. Also defined as a clinical method for evaluating the stage of skeletal maturation of a child, hence it is also called as skeletal age assessment. Skeletal maturity gives the measure of development of a bone incorporating its shape, size and degree of mineralization [1]. Bone age assessment is used to determine the difference between skeletal bone age and the chronological age. In normal conditions, the bone age should be approximately 10% of chronological age [1]. The difference between two ages, i.e. bone age and chronological age, shows that there are abnormalities in the skeletal growth of children or there is a hormonal imbalance.

The most important methods for the estimation of age based on radiological analysis were defined by Greulich and Pyle (GP method) [2] and Tanner and Whitehouse (TW1 method) [3] respectively. GP method is an atlas matching method, and is still the most commonly used technique, because the method is very easy and less time consuming. The TW1 method is more flexible and has been derived from a solid mathematical base. The TW1 method has

been modified throughout the years, evolving to TW3 method [4]. The only difference made was calibrating the scoring method on North American and European children. In TW3 method each bone in region of interest is given a score. An overall score of all these bones is calculated. Overall score indicates to a particular bone age as mentioned in the tables and graphs of TW3 method. The process is complex, so it is seldom used, yet its modular structure makes it suitable for automation. The ages that can be predicted using these methods is in the range of 0–18 years, as after the age of 18 years the bones are completely matured and fusion is complete.

When the hand radiographs are to be processed digitally, one of the problems that occur is non-uniform contrast variation of the background. This is an intrinsic effect in the process of digital acquisition of radiograph. It poses a major challenge to the segmentation algorithm along with the problem of pixel intensity overlapping between bone and soft tissue region. Various methods have been designed to remove the background of radiograph as pre-processing [5,6]. The most challenging part is removal of soft tissue region. In order to solve the problem, image segmentation techniques are required. Image segmentation techniques can be classified into, thresholding, clustering, edge-based, region-based, deformable models and hybrid techniques.

Thresholding is the oldest and first segmentation technique, also the most widely applied segmentation technique. It presumes that both foreground and background regions have mutually exclusive range of pixel intensities. Segmenting the bones from soft tissue

\* Corresponding author.

E-mail addresses: [shreyas.simu@gmail.com](mailto:shreyas.simu@gmail.com) (S. Simu), [\(S. Lal\)](mailto:shyam.mtec@gmail.com).

region can be achieved by Sobel gradient [5,7]. This method has limitations as the gradient image can't be further used for segmentation. Also overlapping of pixels is present in the resulting image. Similar segmentation techniques like Derivative of Gaussian (DoG) and dynamic thresholding have also been implemented on hand radiographs [8–10]. But these techniques hold the same problems as the previous technique. Otsu thresholding which is based on maximizing the inter class variance was implemented on hand radiographs, but the major problem with the technique was that results were not accurate [11,12].

Clustering is an unsupervised learning strategy that groups similar patterns into clusters. Most popular clustering technique used for segmentation is k-means clustering technique wherein the pixels are classified into k clusters, based on distance measure such as Euclidean distance. Clustering process depends upon optimization of an objective function, such as minimization of a squared error function. Adaptive clustering algorithm based on k-means clustering along with Gibbs random fields was formulated by Pappas [13]. This clustering technique was implemented on hand radiographs by many researchers, but the results were appalling as it was not effective on slowly varying textures, [14–17]. The k-means clustering algorithm along with gray-level co-occurrence matrix was used by Chai et al. for segmentation [18]. The drawbacks were that number of gray levels had to be manually decided and it was computationally intensive and time consuming.

Edges are pixels which go through a sudden change in gray level intensity, also known as discontinuities. These edges are connected into a closed boundary and the pixels inside this closed boundary are called objects. This technique is referred as edge-based segmentation. Region-based segmentation techniques segment an image by classifying it into two sets of pixels, foreground and background. The theory behind this technique is that the region to be segmented has similar image properties such as analogous range of pixel intensities, texture and pattern [19]. Region growing and region merging technique was applied by Manos et al. on hand radiographs [20]. This technique is insensitive to image semantics and is unable to separate multiple disconnected objects simultaneously.

A class of techniques that generates an approximate model of the targeted object using some prior information is called as deformable models. The prior information used to create a model can be edge information, shape of an object or image texture. Three major classes of deformable models arise from the type of prior information used, they are active contour model (edge information) (ACM), active shape model (shape information) (ASM) and active appearance model (image texture) (AAM) [21]. Niemeijer et al. had segmented middle phalanx of the third finger using ASM [22]. The dataset consisted of images of age group 9–17 years. Other authors also tried using ASM and ACM for segmentation [23]. Thodberg et al. proposed a complete BAA system called as BoneXpert method [24]. The bone reconstruction is based on AAM. However the age groups 17–18 and 0–2 were omitted from the dataset. Also radius and ulna bones were poorly reconstructed.

Hybrid techniques are basically combination of two or more aforementioned techniques. Watershed algorithm is a classic example of hybrid segmentation technique. It is based on the basic concepts thresholding, region growing and edge detection techniques. Han et al. implemented it on hand radiographs but it had limitations due to sensitivity towards noise and heavy dependence on gradient of the image [25]. Particle Swarm Optimization was used along with edge detectors [26] and also with graph-based segmentation [27]. The drawback of PSO is that the solution sometimes gets cornered in a local optimum. Hence it might work well in some situations but might fail in other.

This paper focuses on comparison between various evolutionary and non-evolutionary segmentation techniques on different hand

radiographs. A sound comparison is done by performing qualitative and quantitative analysis on hand radiographs, which was lacking in the literature. Novelty of paper lies in wide and in-depth analysis done by applying various robust, popular and widely used segmentation techniques on hand radiographs.

The paper is organized as follows: Section 2 discusses the various non-evolutionary and evolutionary segmentation techniques. A brief discussion about methods has been done. In Section 3 we describe the materials and methods. In Section 4 we discuss the results and compare the segmentation results of different evolutionary and non-evolutionary segmentation techniques using standard quality metrics. Finally we conclude the work in Section 5.

## 2. Segmentation techniques

The hand radiograph can be divided into 3 distinct regions namely, background, soft tissue region and the bones. Since composition of radiograph is made of these regions, evaluating segmentation techniques like thresholding and clustering for extraction of bones on the radiograph is justified. There have been several techniques devised for segmentation of image based on multi-level thresholding. We have covered some of the popular thresholding techniques namely, Otsu's thresholding [11] and Tsallis entropy based thresholding [28]. Other segmentation techniques covered in this paper include, adaptive clustering algorithm based on k-means clustering with Gibbs random fields (KGRF) [13], adaptively regularized kernel-based fuzzy C-means clustering (ARKFCM) [29], k-means clustering using GLCM [18] and bi-convex fuzzy variational image segmentation method [30]. The previous mentioned segmentation techniques can be classified as non-evolutionary segmentation techniques. Whereas optimization techniques used for multi-level thresholding are classified as evolutionary segmentation techniques, such as Particle Swarm Optimization (PSO) [31] and Darwinian PSO (DPSO) [32]. Multiplicative intrinsic component optimization (MICO) technique [33] was recently developed for MRI image segmentation has been also explored. MICO is based on estimating the bias field and simultaneously segmenting the required regions.

### 2.1. Non-evolutionary segmentation techniques

#### 2.1.1. Segmentation based on Otsu's thresholding method

Thresholding using Otsu's method, we try to find a threshold value that minimizes the intra class variance  $\sigma_w^2(t_h)$  given by the weighted sum of variances of the two classes [11]:

$$\sigma_w^2(t_h) = \omega_1(t_h)\sigma_1^2(t_h) + \omega_2(t)\sigma_2^2(t) \quad (1)$$

where  $\omega_i(t_h)$  are probabilities of two classes separated by threshold  $t_h$ . Otsu has shown that minimizing the intra class variance is equivalent to maximizing the inter-class variance  $\sigma_b^2(t_h)$ :

$$\sigma_b^2(t_h) = \sigma^2(t) - \sigma_w^2(t_h) = \omega_1(t_h)\omega_2(t_h)[\mu_1(t_h) - \mu_2(t_h)]^2 \quad (2)$$

which is given in terms of class probability  $\omega_i(t_h)$  and class mean  $\mu_i(t_h)$ . The class probability  $\omega_i(t)$  is calculated from histogram:

$$\omega_1(t_h) = \sum_{i=0}^{t_h-1} p(i) \quad (3)$$

$$\omega_2(t_h) = \sum_{i=t_h}^{L-1} p(i) \quad (4)$$

while the class mean are:

$$\mu_1(t_h) = \sum_{i=0}^{t_h-1} p(i)x(i) \quad (5)$$

$$\mu_2(t_h) = \sum_{t_h}^{L-1} p(i)x(i) \quad (6)$$

$x(i)$  is the value at center of the  $i$ th histogram and  $L$  is the number of levels in an image.

This algorithm assumes that images contain two classes of pixels resulting in bimodal histogram (foreground and background). It calculates the optimum threshold which separates the two classes so that the combined spread is minimal. The extension of this is multi-level thresholding called as multi-Otsu [11].

**Algorithm 1.** Algorithm for segmentation using Otsu's thresholding method

- Step 1** Calculate the histogram and probabilities at each intensity level from 0 to  $L-1$ .
- Step 2** Initialize  $\omega_i(0)$  and  $\mu_i(0)$ .
- Step 3** Iterate through all threshold values from  $t=1$  to maximum intensity value.
- Step 4** Compute  $\sigma_b^2(t_h)$ .
- Step 5** Required threshold value corresponds to the maximum value of  $\sigma_b^2(t_h)$ .

#### 2.1.2. Segmentation based on Tsallis entropy

de Albuquerque et al. proposed a segmentation technique based on Tsallis entropy [28]. Consider an image with  $l$  gray levels. The probability distribution of the levels is given by  $p_i = p_1, p_2, \dots, p_l$ . We divide this distribution into two probability distributions, one for foreground and another for background [28]. The probability distributions of the foreground and background classes, called A and B respectively, are given by:

$$p_A = \frac{p_1}{P^A}, \frac{p_2}{P^A}, \dots, \frac{p_{t_h}}{P^A} \quad \text{and} \quad p_B = \frac{p_{t_h+1}}{P^B}, \frac{p_{t_h+2}}{P^B}, \dots, \frac{p_l}{P^B} \quad (7)$$

where  $P^A = \sum_{i=1}^{t_h} p(i)$  and  $P^B = \sum_{i=t_h+1}^l p(i)$ .

For each distribution the a priori Tsallis entropy is defined as:

$$E_x^A(t_h) = \frac{1 - \sum_{i=1}^{t_h} (p_i/p^A)^x}{x-1} \quad \text{and} \quad E_x^B(t_h) = \frac{1 - \sum_{i=t_h+1}^l (p_i/p^B)^x}{x-1} \quad (8)$$

The entropic index  $x$  distinguishes the degree of nonextensivity. Tsallis entropy  $E_x(t_h)$  relies on the threshold value  $t_h$  for the division into foreground and background regions [28]. It is generalized as the sum of each entropy:

$$E_x(t_h) = \frac{1 - \sum_{i=1}^{t_h} (p_A)^x}{x-1} + \frac{1 - \sum_{i=t_h+1}^l (p_B)^x}{x-1} + (1-x) \cdot \frac{1 - \sum_{i=1}^{t_h} (p_A)^x}{x-1} \cdot \frac{1 - \sum_{i=t_h+1}^l (p_B)^x}{x-1} \quad (9)$$

When  $E_x(t_h)$  is maximized, the value of  $t_h$  is considered to be the optimum threshold value. This can be achieved by optimizing the objective function [28]:

$$t_{hopt} = \arg \max [E_x^A(t_h) + E_x^B(t_h) + (1-x) \cdot E_x^A(t_h) \cdot E_x^B(t_h)] \quad (10)$$

The above process can be easily extended to multi-level thresholding.

**Algorithm 2.** Algorithm for segmentation using Tsallis entropy

- Step 1** Divide the image into foreground and background and calculate the probability distribution of each intensity level given by Eq. (7).
- Step 2** Calculate the Tsallis entropy for each region using Eq. (8).
- Step 3** Maximize the objective function given in Eq. (10).
- Step 4** Iterate through all threshold values from  $t_h=1$  to maximum intensity value.

#### 2.1.3. Segmentation using adaptive clustering algorithm based on k-means clustering with Gibbs random fields

This segmentation algorithm consists of two stages. First stage is clustering using the k-means algorithm and second stage is using Gibbs random fields for estimation of the intensity function segmentation.

The k-means algorithm uses the Euclidean distance  $s$  between samples and cluster centers  $c$  to calculate the similarity. Each pixel  $o$  can be identified by three values, it's image coordinates and the gray level intensity value. Using this algorithm the samples are clubbed together into a predefined number of classes  $n$ . This classification is completely based on the minimization of difference between sample and cluster centers [19].

In the second stage we assign the image pixels to one of the classes based on their intensity and relative location. Let the intensity of pixel  $o$  located at  $i$  be denoted as  $o_i$ . We denote segmentation of image into classes by  $x$ , where  $x_i = z$ ,  $z$  is one of the class among  $n$  number of classes. We assume that every class is a slowly varying intensity function. Gibbs random model fields are used for spatial information which describe the local distribution of gray levels. The probability density function is now defined as:

$$p(x_i|g, x_q \text{ for all } q \neq i) = p(x_i|g_i, x_q, q \in W_i) \propto \exp \times \left( -\frac{1}{2\sigma^2} [g_i - \mu_i^{(x_i)}]^2 - \sum_{x_i \in C} V_C(x) \right) \quad (11)$$

where  $q$  is the clique pixel,  $\mu_i$  is a gray level of intensity function for each class  $x_i$ ,  $g_i$  is the pixel gray level value,  $\sigma^2$  is the noise variance,  $W_i$  is a window size around pixel  $i$ ,  $V_C$  is a clique potential in Gibbs model.

The intensities values are updated continuously by averaging gray level values of pixels belonging to the considered classes in the sliding window whose size is decreased in every iteration. The algorithm maximizes this probability density function and estimates the intensity functions, interchangeably. A more detailed description of this segmentation algorithm can be found in [13,14].

The two-point and one-point clique potentials are defined as:

$$V_C = \{-\lambda, x_i = x_q \quad i, q \in C\} \quad \text{or} \quad V_C = \{+\lambda, x_i \neq x_q \quad i, q \in C\} \quad (12)$$

where  $C$  is the summation of all clique values in that region. The value clique potential  $\lambda$  is set to 0.5. A negative value of  $\lambda$  says that two pixels do not belong to same class [13].

**Algorithm 3.** Clustering algorithm based on KGRF

- Step 1** Perform k-means clustering on the given image.
- Step 2** Initialize the window size  $W$  to the size of image and number of iterations  $m$  to 1.
- Step 3** Estimate the value of  $\mu_i$ .
- Step 4** From the new value of  $\mu_i$ , perform k-means segmentation,  $m = m + 1$ .
- Step 5** Repeat steps 3 and 4 till  $m = m_{max}$ . When value of  $m = m_{max}$  reduce the window size  $W$  and repeat steps 3 and 4.
- Step 6** If window size  $W = W_{min}$  terminate the algorithm.

### 2.1.4. GLCM based adaptive crossed reconstruction (ACR)

#### k-means clustering for segmentation

Chai et al. proposed segmentation using gray level co-occurrence matrix and k-means clustering algorithm [18]. The GLCM is used for texture analysis which was proposed by Haralick [34]. In this method the image is first divided into number of vertical and horizontal bands. Unsupervised k-means clustering is then applied with  $k=2$  and  $k=3$  on the sub-image. The contrast and homogeneity values of these images are found using GLCM. Maximum value of homogeneity is checked and the sub-images which give highest values are thus used to reconstruct the image.

#### Algorithm 4. GLCM based ACR k-means algorithm

- Step 1** Divide the image into pre-defined number of vertical bands.
- Step 2** Divide the resulting images into pre-defined number of horizontal bands.
- Step 3** Perform k-means clustering on each sub-image with  $k=2$  and  $k=3$ .
- Step 4** Perform texture analysis on resulting sub-images using GLCM defined by Haralick [34].
- Step 5** Check the contrast and homogeneity values of these GLCM results.
- Step 6** Use only those images which give highest homogeneity values for reconstruction of images.

### 2.1.5. Segmentation based on adaptively regularized kernel-based fuzzy C-means clustering (ARKFCM) algorithm

The fuzzy C-means (FCM) algorithm from which ARKFCM has been designed, assigns a membership value to each pixel for all clusters in the image space [35]. Assume an image  $I$  with set of grayscale values  $x_i$  at pixel  $i$  ( $i=1, 2, \dots, N$ ), where  $N$  is total number of pixels.  $X = x_1, x_2, \dots, x_N$  in  $k$ -dimensional space and with cluster centers  $d = d_1, d_2, \dots, d_c$  where  $c$  being a positive integer ( $2 < c \ll N$ ), there is a membership value  $u_{ij}$  for each pixel  $i$  in the  $j$ th cluster ( $j=1, 2, \dots, c$ ). The objective function of the FCM algorithm is [35]

$$O_{\text{FCM}} = \sum_{i=1}^N \sum_{j=1}^c u_{ij}^q \|x_i - d_j\|^2 \quad (13)$$

where  $q$  is a weighting exponent to the degree of fuzziness, i.e.  $q > 1$ , and  $\|x_i - d_j\|^2$  is the gray-scale Euclidean distance between pixel  $i$  and center  $d_j$ . The FCM algorithm is very sensitive to noise and the accuracy decreases in the presence of noise.

Elazab et al. [29] have introduced an adaptive regularization parameter  $\lambda$ , to enhance segmentation robustness, also devise a weighted image, and adopt the Gaussian radial basis function (GRBF) for better accuracy.

The objective function is defined as:

$$O_{\text{ARKFCM}} = 2 \left[ \sum_{i=1}^N \sum_{j=1}^c u_{ij}^q (1 - K(x_i, d_j)) + \sum_{j=1}^c \lambda_j u_{ij}^q (1 - K(\bar{x}_i, d_j)) \right] \quad (14)$$

where  $x_i$  can be an average (ARKFCM-avg) or median (ARKFCM-med) filtered or a weighted (ARKFCM-wtd) image. In the above objective function, a GRBF kernel  $K$  is used instead of Euclidean distance measure:

$$\|\lambda(x_i) - \lambda(d_j)\|^2 = 2(1 - K(x_i, d_j)) \quad (15)$$

where  $K$  is kernel function with width  $\omega$ :

$$K(x_i, d_j) = \exp \left( \frac{\|x_i - d_j\|^2}{2\omega^2} \right) \quad (16)$$

For detailed mathematical analysis refer to [29].

#### Algorithm 5. ARKFCM algorithm

- Step 1** Initialize loop counter  $t=0$ , and other variables  $d, u$  and  $\lambda$ .
- Step 2** Calculate  $\bar{x}_i$  based type of filtering average, median or weighted image.
- Step 3** Calculate the cluster centers  $d_i$  using equation:

$$d_j = \frac{\sum_{i=1}^N u_{ij}^q (K(x_i, d_j)x_i + \lambda_i K(\bar{x}_i, d_j)\bar{x}_i)}{\sum_{i=1}^N u_{ij}^q (K(x_i, d_j) + \lambda_i K(\bar{x}_i, d_j))} \quad (17)$$

- Step 4** Calculate the membership function  $u_{ij}$  using equation:

$$u_{ij} = \frac{((1 - K(x_i, d_j) + \lambda_i(1 - K(\bar{x}_i, d_j)))^{-(1/(q-1))}}{\sum_{i=1}^c ((1 - K(x_i, d_j) + \lambda_i(1 - K(\bar{x}_i, d_j)))^{-(1/(q-1))}} \quad (18)$$

- Step 5** If maximum number of iteration are over then stop, otherwise, update  $t=t+1$  and go to step (3).

### 2.1.6. Segmentation based on bi-convex fuzzy variational (BFV) image segmentation algorithm:

This algorithm combines fuzzy logic with Chan-Vese (CV) model [36] to make a bi-convex objective function. CV model belongs to the class of partial differential equation (PDE) model equations for solving image segmentation problems. There have been three major problems with CV model, viz. (1) convergence to local optima, (2) highly dependent on parameter selection, and (3) computationally expensive. Whereas BFV algorithm [30] efficiently combines numerical remedy techniques and lengthly penalty terms to give better results. Thus reducing the computational costs and also bringing a lot of robustness to parameter settings.

The fuzzy energy function used is:

$$E = w_1 \int_R u^m (I - b_1)^2 dx + w_2 \int_R (1 - u)^m (I - b_2)^2 dx \quad (19)$$

where  $u$  is the membership function,  $m$  is a constant positive integer,  $w_1, w_2$  are weights and  $b_1, b_2$  are average values of given image  $I$  inside and outside the curve  $\gamma$ .

#### Algorithm 6. Bi-convex fuzzy variational algorithm

- Step 1** Initialize  $b_1, b_2$ , and  $u$  randomly to calculate  $g(r(|\nabla I|, S))$ :

$$g(x, S) = \epsilon(S - S_0)e^{-x^2} + (1 - \epsilon(S - S_0)) \frac{1}{1+x^2} \quad (20)$$

$$r(|\nabla I|, S) = \epsilon(S - S_0)|\nabla I| + (1 - \epsilon(S - S_0))|G * \nabla I| \quad (21)$$

where  $S$  is the SNR of test image,  $\epsilon(S) = (1/(1+e^{-S}))$ ,  $G$  is a Gaussian kernel.

- Step 2** Calculate  $b_1$  and  $b_2$  using equations:

$$b_1 = \frac{\int_R u^m I dx}{\int_R u^m dx} \quad \text{and} \quad b_2 = \frac{\int_R (1-u)^m I dx}{\int_R (1-u)^m dx} \quad (22)$$

- Step 3** Set  $t_1 = 0$ . Calculate  $u_{n+1/2}$  using equation:

$$\frac{\partial u}{\partial t} = m(-w_1 u^{m-1} (I - b_1)^2 + w_2 (1 - u)^{m-1} (I - b_2)^2) \quad (23)$$

If  $t_1 + \Delta t_1 \leq T_1$  then  $t_1 = t_1 + \Delta t_1$ ,  $u^n = u^{n+1/2}$  and move to step 2, else continue.

- Step 4** Calculate  $u_{n+1}$  using equation:

$$u_n = u_{n+1/2} + \Delta t_2 g(r(|\nabla I|, S), S) \Delta u_{n+1/2} \quad (24)$$

**Step 5** If  $u_{n+1}$  satisfies stationary condition then stop, otherwise go to step 2.

There are two stationary conditions, one is predefined number of iterations and other is  $\max|u_{n+1} - u_1| \leq \varepsilon$  where  $\varepsilon$  is any small positive constant.

## 2.2. Evolutionary segmentation techniques

### 2.2.1. Segmentation based on PSO algorithm

Eberhart and Kennedy developed Particle Swarm Optimization algorithm in which the contestant solutions are known as particles. At every step, a fitness function is evaluated to find the particle success [31]. Eqs. (25) and (26) show how each particle  $i$  navigates through a space based on the position  $x_i$  and velocity  $v_i$  values which rely on local best ( $lbest$ ), and global best ( $gbest$ ) information.

The PSO algorithm evaluates each particle for the fitness function, which is defined as the inter-class variance given in Eq. (1). The local and global best values are initialized with the random possible values. Population size and stopping criteria are the other two parameters which need to be adjusted. The population size is very critical factor to optimize and achieve an overall good solution. Based on the problem, stopping criteria can be a predefined number of iterations or any other criteria [37].

**Algorithm 7.** Algorithm for segmentation based on PSO

**Step 1** Particles are randomly generated between the limits of threshold values for a population size  $P$ .

**Step 2** Objective functions of these particles are calculated.

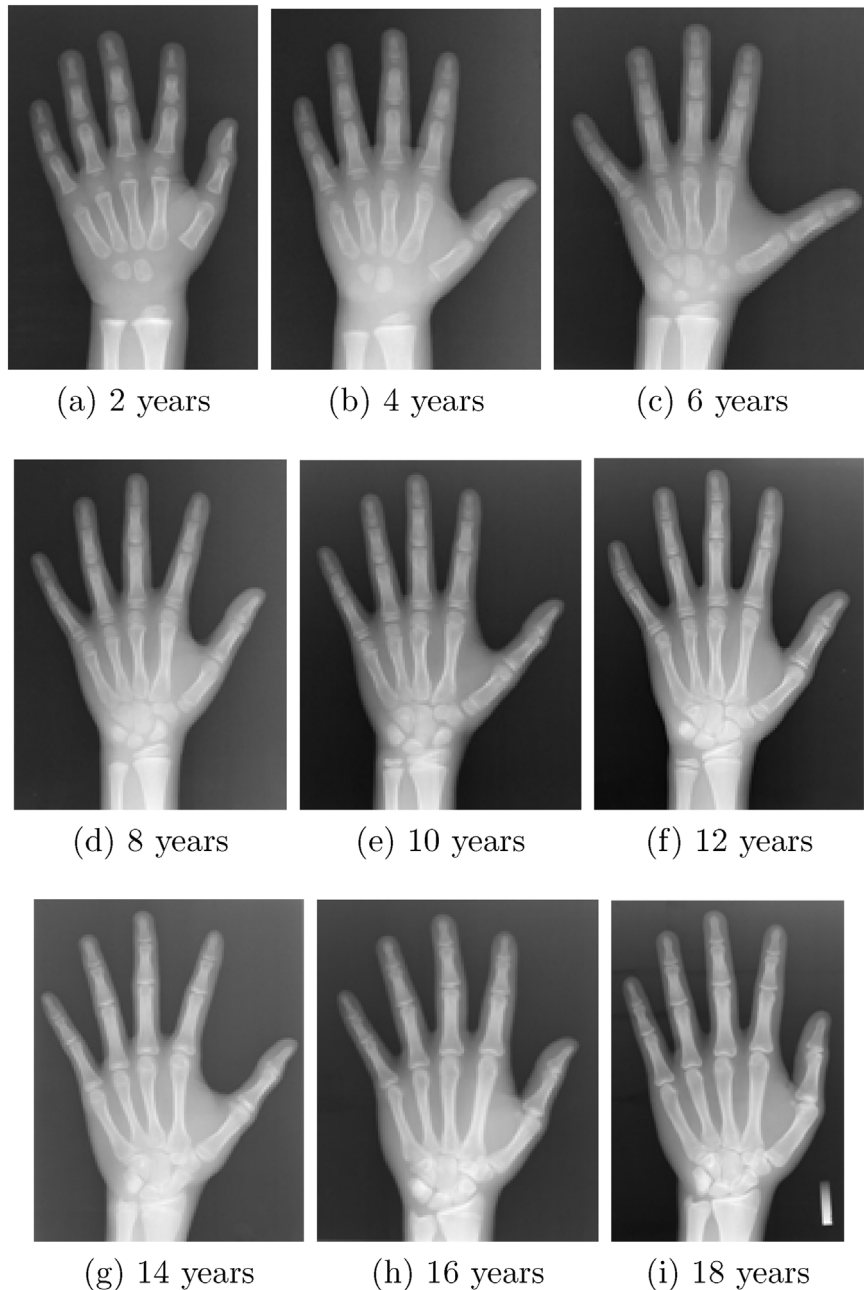


**Fig. 1.** Test radiographs used from the image database.

**Step 3** The values obtained from previous step are used to set the *lbest* and *gbest*.

**Step 4** Velocity is computed using the equation:

$$\begin{aligned} v(i+1) &= v(i) + \lambda_1 * r(i) * (lbest(i) - x(i)) \\ &\quad + \lambda_2 * r(i) * (gbest(i) - x(i)) \end{aligned} \quad (25)$$

where  $\lambda_1$  and  $\lambda_2$  are learning factors and  $r(i)$  is a random number between 0 and 1.

**Step 5** Position of each particle is updated using the equation:

$$x(i+1) = x(i) + v(i+1) \quad (26)$$

**Step 6** Objective functions are calculated for updated values. If the new values is better than the previous value then it is set as *lbest* and *gbest* respectively.

**Step 7** Repeat the above process until stopping criteria is satisfied.

## 2.2.2. Segmentation based on DPSO algorithm

The major drawback of PSO technique is that, solution gets cornered in a local optimum [37]. The concept of Darwinian Particle Swarm Optimization (DPSO) was expressed by Tillet et al. [32]. At a given point of time in DPSO many swarms of test solutions exist. Each of the swarms behave like an ordinary PSO algorithm which uses natural selection to breakout from local optima. If a search gets trapped in a local optimum, the search in that region is discarded and another region is searched. In DPSO, at every step, swarms that improve are rewarded and swarms which hinder are punished [32,37]. The state of each swarm and the fitness of all particles is calculated. The neighborhood and individual best positions of each particle is also updated. A new particle is spawned only if a new global solution arises. Whereas a particle is deleted if the swarm fails to update to a better state in a pre-defined number of iterations [32,37].

**Algorithm 8.** Algorithm for segmentation based on DPSO

**Step 1** Evolve each swarm in the group.

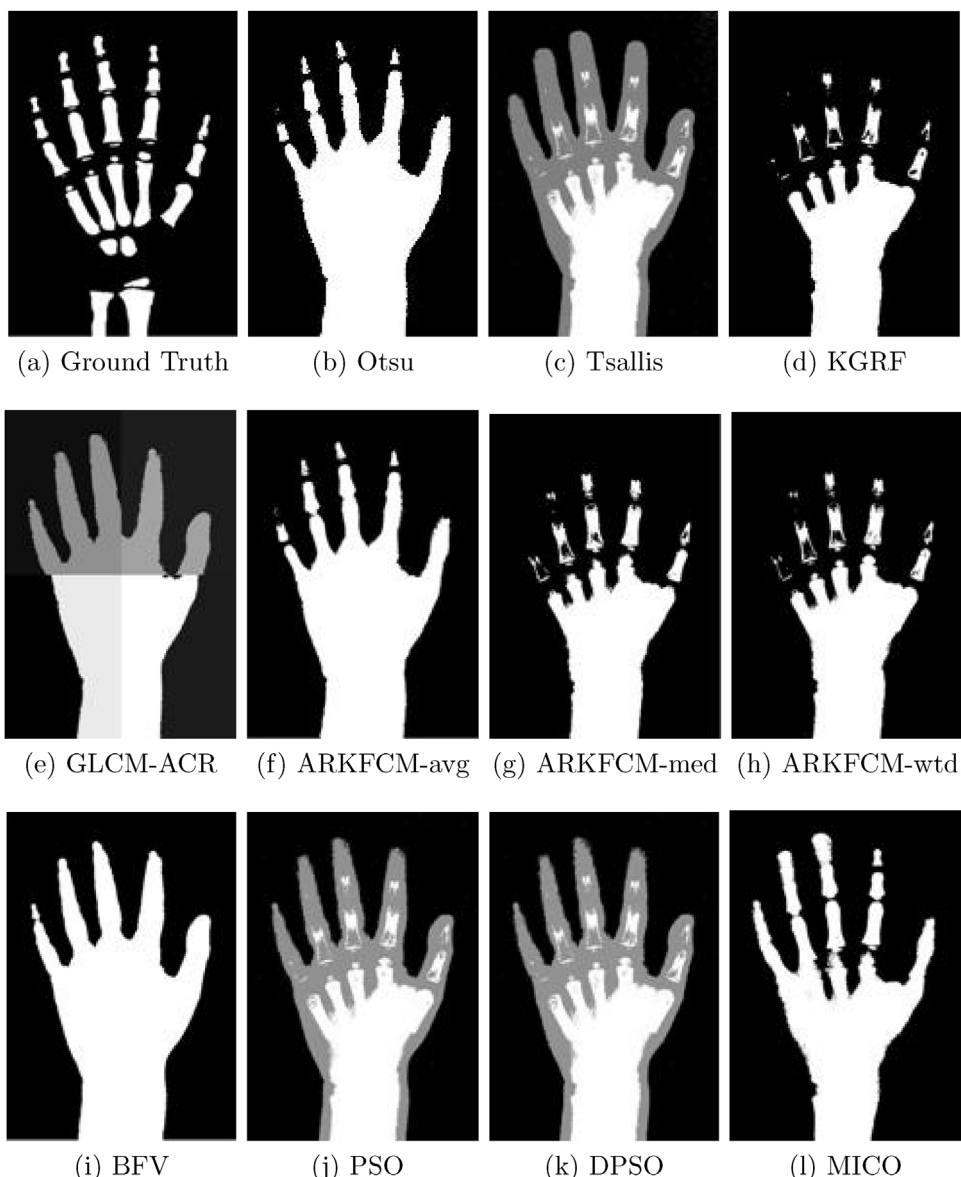


**Fig. 2.** Segmentation results of different algorithms on hand radiograph taken from 2 year old person [5329.jpg].

- Step 2** Update particle fitness and update particle best for each particle.
- Step 3** Update the velocity vector.
- Step 4** Find objective values, check the fitness, if fitness criteria not met, delete the particle.
- Step 5** If the swarm gets better results, reward the swarm (extend swarm life) if not, punish swarm (reduce swarm life or delete). The condition is given by:

$$s_{\min} \leq s \leq s_{\max} \quad (27)$$

where  $s$  is swarm's population,  $s_{\min}$  and  $s_{\max}$  are the minimum and maximum swarm population considered. When the population goes below  $s_{\min}$  swarm is deleted.

- Step 6** Spawn each swarm in the collection.
- Step 7** Delete failed swarms.

### 2.2.3. Multiplicative intrinsic component optimization (MICO)

Li et al. [33] proposed an energy minimization method named as multiplicative intrinsic component optimization (MICO) for bias field estimation and segmentation of MR images. This technique

essentially divides the image into 2 multiplicative components, which are bias field and the true image along with additive noise.

$$M(x) = b(x)I(x) + n(x) \quad (28)$$

The bias field is said to be a linear combination of a set of smooth basis functions  $f_1, \dots, f_m$ . bias field is estimated by finding the optimal coefficients  $w_1, \dots, w_m$ .

$$b(x) = w^T F(x) \quad (29)$$

where  $F(x)$  is a column vector of basis functions  $f_1, \dots, f_m$ . assuming that there are  $N$  types of classes in the image domain  $R$ . Each class is defined by a membership function  $u(i)$ . the true image can be approximated by:

$$I(x) = \sum_{i=1}^N c_i u_i(x) \quad (30)$$

where  $c(i)$  are constants. Thus the energy minimization formulation is given by,

$$E(b, I) = \int_R |M(x) - b(x)I(x)|^2 dx \quad (31)$$

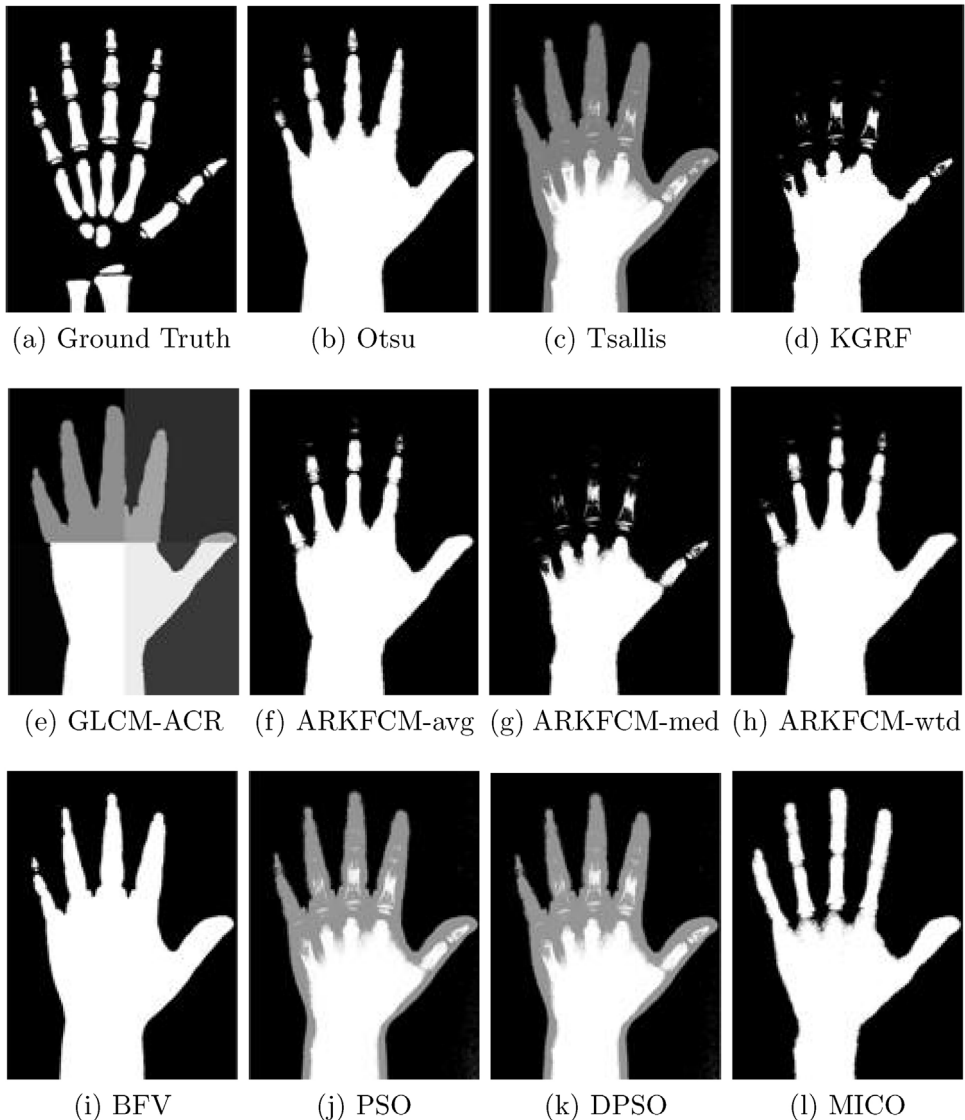


**Fig. 3.** Segmentation results of different algorithms on hand radiograph taken from 4 year old person [5121.jpg].

The energy function  $E(b, I)$  can be articulated in terms of three variables  $u$ ,  $c$  and  $w$  and optimization of  $b$  and  $I$  can be accomplished by minimizing the energy function with respect to these three variables:

$$E_q(u, c, w) = \int_R \sum_{i=1}^N |M(x) - w^T F(x)c_i|^2 u_i^q(x) dx \quad (32)$$

To achieve fuzzy segmentation (soft segmentation) results fuzzifier  $q \geq 1$  has been introduced. For  $q > 1$  the fuzzy membership functions can take value between 0 and 1. Detailed mathematical analysis of energy minimization function can be read in [33].

To achieve energy minimization we need to minimize  $E_q(u, c, w)$  with respect to each variable keeping other two fixed.

**Algorithm 9.** Multiplicative intrinsic component optimization algorithm

**Step 1** Minimize  $E$  with respect to  $w$ , initialize  $c$  and  $u$ .

**Step 2** Update the value of  $b$  according to equation:

$$\hat{b}(x) = \hat{w}^T F(x) \quad (33)$$

**Step 3** Update the value of  $c$  according to the equation:

$$\hat{c}_i = \frac{\int_R M(x)b(x)u_i^q(x)dx}{\int_R b^2(x)u_i^q(x)dx} \quad (34)$$

**Step 4** Update the value of  $u$  according to the equation:

$$\hat{u}_i(x) = \frac{(|M(x) - w^T F(x)c_i|^2)^{1/(1-q)}}{\sum_{j=1}^N (|M(x) - w^T F(x)c_j|^2)^{1/(1-q)}} \quad (35)$$

**Step 5** Check if convergence has been reached or the number of iterations have exceeded, stop the iteration or else go to step 2.

### 3. Materials and methods

#### 3.1. Image database

The database used was acquired from online website, <http://www.ipilab.org/BAAweb/>. The images on this website have been collected from Children's Hospital Los Angeles (CHLA), United States of America. The manual segmentation or ground truth images were constructed with the help of orthopedicians from Goa Medical College (GMC), Bambolim, Goa, India.

In this paper, we have presented results of 9 images taken from the database of Asian male images from the website mentioned previously. Each image selected has age gap of 2 years between the age range of 2–18 years. The TW3 method [4] estimates bone age up to the age of 18 years as after that age the bones of hand are completely matured and there are no significant changes in the shape and structure that can be tracked.

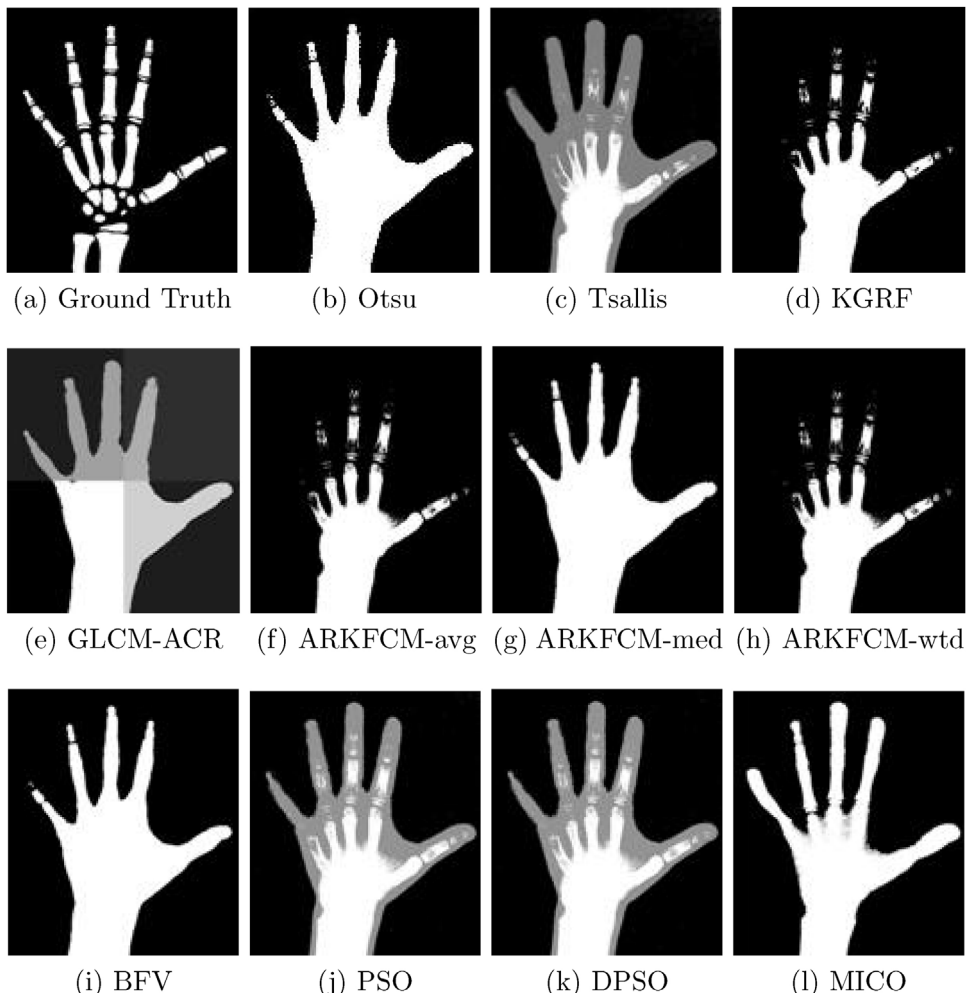


**Fig. 4.** Segmentation results of different algorithms on hand radiograph taken from 6 year old person [5072.jpg].

### 3.2. Segmentation and analysis procedure

The segmentation of bones from hand radiographs and result analysis involves 4 simple steps.

- 1 The hand radiograph of a particular age is read in MATLAB script.
- 2 Anisotropic diffusion is performed on the radiograph image as pre-processing step.
- 3 Segmentation techniques discussed in the previous section are then applied one by one.
- 4 Segmented image and ground truth image is then compared using various image quality metrics.

Before segmentation of the bones we apply anisotropic diffusion. Perona and Malik [38] introduced anisotropic diffusion, which is also called as non-linear anisotropic diffusion. Unlike other isotropic diffusion algorithms used for noise removal, anisotropic diffusion algorithm preserves the edges while diffusing the noise. It will smoothen the image where gradient is less and preserve the high gradient region or edges. This pre-processing step not only helps in noise removal but also makes segmentation of bones easier.

### 3.3. Quantitative performance metrics

The segmentation results have been evaluated using various performance metrics like PSNR and MSE [19], Jaccard similarity index (JSI), structure similarity index (SSIM), dice similarity and accuracy [39]. The computational cost in terms of time taken by CPU for execution of each segmentation technique has also been calculated.

The mathematical expression for PSNR is:

$$\text{PSNR (dB)} = 10 * \log_{10} \left( \frac{255^2}{\text{MSE}} \right) \quad (36)$$

MSE is given by:

$$\text{MSE} = \frac{1}{mn} \sum_{i=1}^m \sum_{j=1}^n (S - G)^2 \quad (37)$$

where  $S$  stands for segmented image and  $G$  for ground truth image. Structure similarity index (SSIM) is given by equation:

$$\text{SSIM}(S, G) = \frac{(2\mu_S\mu_G + \lambda_1)(2\sigma_{SG} + \lambda_2)}{(\mu_S^2 + \mu_G^2 + \lambda_1)(\sigma_S^2 + \sigma_G^2 + \lambda_2)} \quad (38)$$

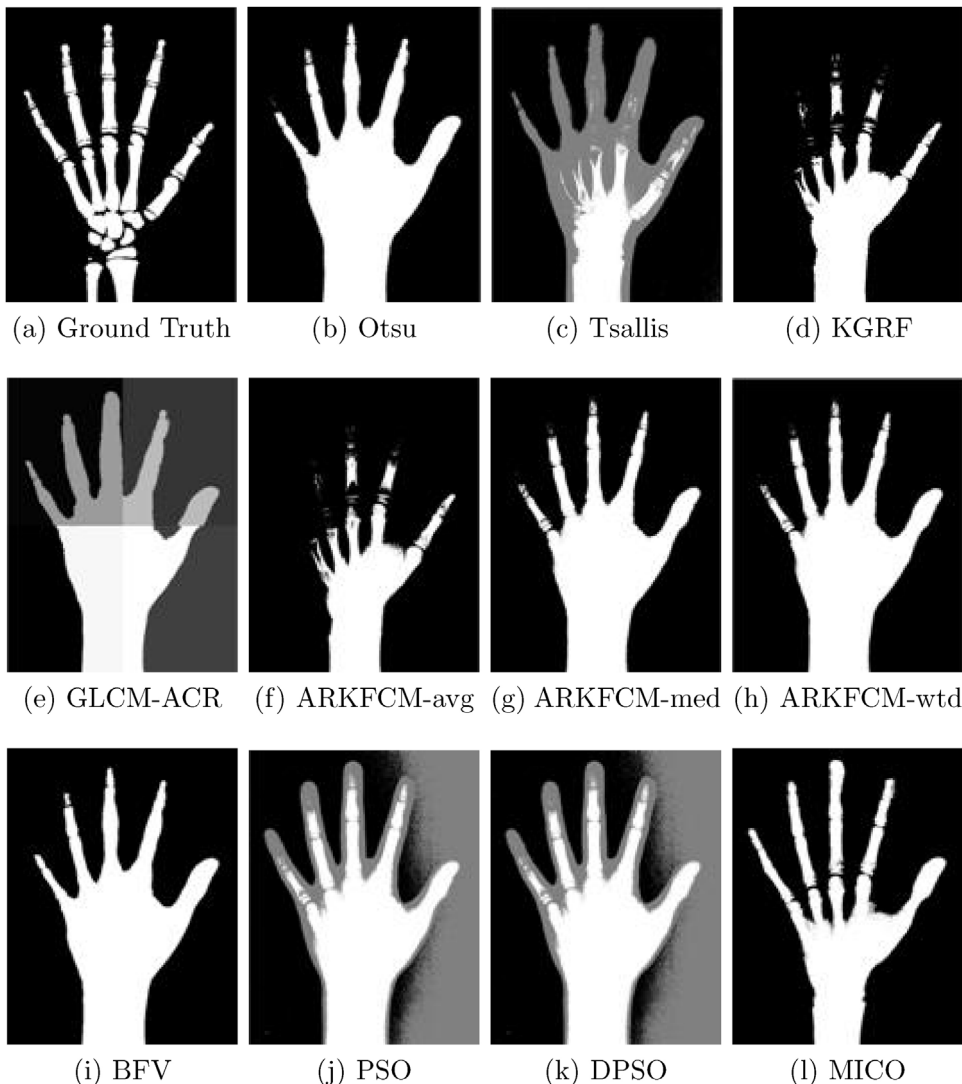


**Fig. 5.** Segmentation results of different algorithms on hand radiograph taken from 8 year old person [5097.jpg].

**Table 1**

Quality metric results for segmentation of hand radiograph taken from 2 year old person [5329.jpg].

Techniques	PSNR	MSE	SSIM	JSI	Dice	ACC	Time(s)
Otsu [11]	46.19	1.56	0.83	0.14	0.19	0.49	2.68
Tsallis [28]	56.90	<b>0.13</b>	<b>0.98</b>	0.41	0.58	0.70	<b>1.18</b>
KGRF [13]	56.90	<b>0.13</b>	<b>0.98</b>	0.42	0.60	0.71	28.56
GLCM-ACR [18]	8.23	9784.99	0.00	0.14	0.00	0.01	16.13
ARKFCM-avg [29]	55.38	0.19	<b>0.98</b>	0.41	0.58	0.71	128.75
ARKFCM-med [29]	56.90	<b>0.13</b>	<b>0.98</b>	0.45	0.62	0.72	124.76
ARKFCM-wtd [29]	<b>56.91</b>	<b>0.13</b>	<b>0.98</b>	0.44	0.61	0.72	127.33
BFV [30]	54.43	0.23	0.97	0.37	0.54	0.68	43.52
PSO [31]	56.90	<b>0.13</b>	<b>0.98</b>	0.41	0.58	0.71	7.02
DPSO [32]	56.90	<b>0.13</b>	<b>0.98</b>	0.41	0.58	0.70	7.02
MICO [33]	56.74	0.14	<b>0.98</b>	<b>0.50</b>	<b>0.66</b>	<b>0.75</b>	23.09

Highlighted value signifies the best result among all algorithms.

where  $\mu_S, \sigma_S$  is the mean and variance of segmented image and  $\mu_G, \sigma_G$  is the mean and variance of ground truth image.  $\sigma_{SG}$  is the covariance and  $\lambda_1, \lambda_2$  are small constants to stabilize the denominator.

Jaccard similarity index (JSI) [39] used for performance analysis,

$$\text{JSI} = \frac{|S \cap G|}{|S \cup G|} \quad (39)$$

Dice similarity [39] is given by equation,

$$\text{Dice} = 2 \frac{|S \cap G|}{|S + G|} \quad (40)$$

Accuracy (ACC) [39] gives information about the ratio of the pixels contained within the segmented region achieved by the test algorithm with the pixels of the manually segmented region. The segmentation accuracy is defined as,

$$\text{ACC} = \frac{t_p + t_n}{t_p + f_p + t_n + f_n} \quad (41)$$

where  $t_p$  = true positive,  $t_n$  = true negative,  $f_p$  = false positive and  $f_n$  = false negative. The range of values taken by quality metrics SSIM, JDI, Dice, ACC is between 0 to 1, where 1 denotes perfect segmentation.

#### 4. Experimental results and discussion

The quantitative and qualitative performance evaluation of different non-evolutionary segmentation techniques such as Otsu's thresholding [11], Tsallis entropy [28], adaptive clustering algorithm based on k-means clustering with Gibbs random fields (KGRF) [13], adaptive crossed reconstruction using GLCM (GLCM-ACR) [18], ARKFCM algorithm [29], BFV algorithm [30] and evolutionary segmentation techniques such as PSO algorithm [31], DPSO algorithm [32], MICO algorithm [33] implemented on digital hand radiographs are discussed in this section. The segmentation results obtained for various digital hand radiographs at ages 2 [5329.jpg (1063 × 1507)], 4 [5121.jpg(1209 × 1616)], 6 [5072.jpg(1558 × 1788)], 8 [5097.jpg(1520 × 1950)], 10 [5217.jpg(1619 × 2018)], 12 [5322.jpg(1592 × 2081)], 14 [5225.jpg(1910 × 2419)], 16 [5208.jpg(1841 × 2248)] and 18 [6145.jpg(1616 × 2376)] are given in Tables 1–9.

All segmentation results were obtained on a 64-bit system with MATLAB 2015a software, having a 4 GB RAM and an Intel i7 processor with clock speed of 2.93 GHz.

##### 4.1. Quantitative analysis

The quantitative analysis of various evolutionary and non-evolutionary segmentation techniques using the quality metrics discussed is presented in tabular form. Tables 1–9 show the

**Table 2**

Quality metric results for segmentation of hand radiograph taken from 4 year old person [5121.jpg].

Techniques	PSNR	MSE	SSIM	JSI	Dice	ACC	Time(s)
Otsu [11]	46.23	1.55	0.83	0.15	0.20	0.49	2.67
Tsallis [28]	<b>56.59</b>	<b>0.14</b>	<b>0.98</b>	0.37	0.54	0.69	<b>1.89</b>
KGRF [13]	56.50	0.15	<b>0.98</b>	0.39	0.57	0.70	34.90
GLCM-ACR [18]	7.34	12003.50	0.00	0.15	0.00	0.01	9.33
ARKFCM-avg [29]	55.82	0.17	<b>0.98</b>	0.44	0.61	0.72	151.23
ARKFCM-med [29]	56.52	<b>0.14</b>	<b>0.98</b>	0.39	0.57	0.70	166.00
ARKFCM-wtd [29]	55.82	0.17	<b>0.98</b>	0.44	0.61	0.72	157.75
BFV [30]	54.71	0.22	0.97	0.40	0.57	0.70	51.17
PSO [31]	56.52	<b>0.14</b>	<b>0.98</b>	0.40	0.57	0.70	7.71
DPSO [32]	<b>56.53</b>	<b>0.14</b>	<b>0.98</b>	0.40	0.57	0.70	7.72
MICO [33]	56.19	0.16	<b>0.98</b>	<b>0.48</b>	<b>0.65</b>	<b>0.74</b>	31.64

Highlighted value signifies the best result among all algorithms.

**Table 3**

Quality metric results for segmentation of hand radiograph taken from 6 year old person [5072.jpg].

Techniques	PSNR	MSE	SSIM	JSI	Dice	ACC	Time(s)
Otsu [11]	46.59	1.43	0.84	0.14	0.20	0.50	3.47
Tsallis [28]	58.00	<b>0.10</b>	<b>0.99</b>	0.43	0.60	0.72	<b>1.35</b>
KGRF [13]	<b>58.37</b>	0.09	<b>0.99</b>	0.51	0.68	0.76	52.35
GLCM-ACR [18]	8.32	9578.28	0.00	0.14	0.00	0.01	12.70
ARKFCM-avg [29]	58.33	<b>0.10</b>	<b>0.99</b>	0.51	0.67	0.75	221.25
ARKFCM-med [29]	56.62	0.14	0.98	0.50	0.66	0.75	230.36
ARKFCM-wtd [29]	58.34	<b>0.10</b>	<b>0.99</b>	0.51	0.67	0.75	227.51
BFV [30]	56.64	0.14	0.98	0.50	0.66	0.75	75.46
PSO [31]	58.32	<b>0.10</b>	<b>0.99</b>	0.51	0.67	0.75	9.04
DPSO [32]	58.30	<b>0.10</b>	<b>0.99</b>	0.50	0.67	0.75	9.19
MICO [33]	57.56	0.11	<b>0.99</b>	<b>0.55</b>	<b>0.71</b>	<b>0.78</b>	38.02

Highlighted value signifies the best result among all algorithms.

**Table 4**

Quality metric results for segmentation of hand radiograph taken from 8 year old person [5097.jpg].

Techniques	PSNR	MSE	SSIM	JSI	Dice	ACC	Time(s)
Otsu [11]	46.75	1.37	0.84	0.16	0.22	0.51	3.93
Tsallis [28]	57.88	0.11	<b>0.99</b>	0.43	0.61	0.72	<b>2.66</b>
KGRF [13]	58.28	0.10	<b>0.99</b>	0.53	0.70	0.77	52.82
GLCM-ACR [18]	7.56	11401.31	0.00	0.16	0.00	0.01	13.21
ARKFCM-avg [29]	58.24	0.10	<b>0.99</b>	0.52	0.69	0.76	227.57
ARKFCM-med [29]	57.47	0.12	<b>0.99</b>	0.57	0.73	0.78	246.83
ARKFCM-wtd [29]	57.47	0.12	<b>0.99</b>	0.57	0.73	0.78	228.04
BFV [30]	57.03	0.13	0.98	0.55	0.71	0.78	74.02
PSO [31]	57.66	0.11	<b>0.99</b>	0.58	0.73	0.79	10.53
DPSO [32]	57.70	0.11	<b>0.99</b>	0.58	0.73	0.79	10.38
MICO [33]	<b>59.68</b>	<b>0.07</b>	<b>0.99</b>	<b>0.69</b>	<b>0.82</b>	<b>0.85</b>	44.73

Highlighted value signifies the best result among all algorithms.

**Table 5**

Quality metric results for segmentation of hand radiograph taken from 10 year old person [5217.jpg].

Techniques	PSNR	MSE	SSIM	JSI	Dice	ACC	Time(s)
Otsu [11]	46.74	1.38	0.84	0.17	0.23	0.51	3.85
Tsallis [28]	57.88	0.11	0.99	0.44	0.61	0.72	<b>2.36</b>
KGRF [13]	57.65	0.11	0.99	0.60	0.75	0.80	60.35
GLCM-ACR [18]	8.70	8775.48	0.01	0.17	0.00	0.01	14.72
ARKFCM-avg [29]	57.58	0.11	0.99	0.60	0.75	0.80	250.07
ARKFCM-med [29]	58.59	0.09	0.99	0.54	0.70	0.77	289.81
ARKFCM-wtd [29]	57.59	0.11	0.99	0.60	0.75	0.80	267.66
BFV [30]	57.15	0.13	0.98	0.57	0.73	0.79	86.98
PSO [31]	58.96	0.08	0.99	0.59	0.74	0.79	11.15
DPSO [32]	58.96	0.08	0.99	0.59	0.74	0.79	11.63
MICO [33]	<b>60.84</b>	<b>0.05</b>	<b>0.99</b>	<b>0.76</b>	<b>0.86</b>	<b>0.88</b>	48.45

Highlighted value signifies the best result among all algorithms.

segmentation results for hand radiographs of ages 2, 4, 6, 8, 10, 12, 14, 16 and 18 respectively.

Table 1 shows that PSNR value of ARKFCM-weighted algorithm is highest, with Tsallis, KGRF, PSO, DPSO and MICO

**Table 6**

Quality metric results for segmentation of hand radiograph taken from 12 year old person [5322.jpg].

Techniques	PSNR	MSE	SSIM	JSI	Dice	ACC	Time(s)
Otsu [11]	46.57	1.43	0.84	0.18	0.24	0.51	<b>4.07</b>
Tsallis [28]	57.90	0.11	<b>0.99</b>	0.63	0.77	0.81	5.56
KGRF [13]	58.02	0.10	<b>0.99</b>	0.63	0.78	0.82	63.87
GLCM-ACR [18]	7.59	11324.66	0.00	0.18	0.00	0.01	13.89
ARKFCM-avg [29]	57.73	0.11	<b>0.99</b>	0.62	0.76	0.81	254.04
ARKFCM-med [29]	57.73	0.11	<b>0.99</b>	0.62	0.76	0.81	256.33
ARKFCM-wtd [29]	57.73	0.11	<b>0.99</b>	0.62	0.76	0.81	292.08
BFV [30]	56.60	0.14	0.98	0.56	0.72	0.78	86.15
PSO [31]	58.29	0.10	<b>0.99</b>	0.64	0.78	0.82	11.22
DPSO [32]	58.33	0.10	<b>0.99</b>	0.64	0.78	0.82	13.47
MICO [33]	<b>59.28</b>	<b>0.08</b>	<b>0.99</b>	<b>0.70</b>	<b>0.82</b>	<b>0.85</b>	49.37

Highlighted value signifies the best result among all algorithms.

algorithm having closer values. But JSI, Dice and accuracy values which denote the segmentation quality and accuracy are highest for MICO algorithm. Segmentation accuracy is lowest for GLCM-ACR algorithm. The time taken for segmentation is lowest for Tsallis algorithm and highest for ARKFCM algorithms. In Table 2 we see that PSNR values of PSO, DPSO, Tsallis, KGRF, ARKFCM-median, MICO algorithms are comparable with DPSO being highest among them. Structural similarity (SSIM) values are similar for these algorithms but JSI, Dice and accuracy values are highest for

**Table 7**

Quality metric results for segmentation of hand radiograph taken from 14 year old person [5225.jpg].

Techniques	PSNR	MSE	SSIM	JSI	Dice	ACC	Time(s)
Otsu [11]	46.71	1.39	0.84	0.19	0.26	0.51	5.54
Tsallis [28]	58.34	0.10	0.99	0.65	0.79	0.82	<b>2.64</b>
KGRF [13]	58.75	0.09	0.99	0.65	0.79	0.82	85.69
GLCM-ACR [18]	6.09	16005.70	0.00	0.19	0.00	0.01	20.38
ARKFCM-avg [29]	57.34	0.12	0.98	0.61	0.76	0.81	399.46
ARKFCM-med [29]	57.34	0.12	0.98	0.61	0.76	0.81	388.03
ARKFCM-wtd [29]	57.34	0.12	0.98	0.61	0.76	0.81	371.62
BFV [30]	57.13	0.13	0.98	0.60	0.75	0.80	133.63
PSO [31]	58.75	0.09	0.99	0.65	0.78	0.82	14.34
DPSO [32]	58.79	0.09	0.99	0.65	0.78	0.82	14.16
MICO [33]	<b>60.84</b>	<b>0.05</b>	<b>0.99</b>	<b>0.77</b>	<b>0.87</b>	<b>0.89</b>	419.16

Highlighted value signifies the best result among all algorithms.

MICO algorithm. Tsallis algorithm has least computational cost with Otsu's thresholding method being second highest and ARKFCM algorithms taken the maximum time.

Table 3 has results derived from hand radiograph of 6 year old person and shows that segmentation accuracy metrics are highest for MICO algorithm. The time taken by Tsallis algorithm is least and ARKFCM being highest. There is a huge time difference between the two. Otsu's thresholding algorithm takes closer time value to Tsallis algorithm followed by PSO, DPSO, GLCM-ACR and MICO.

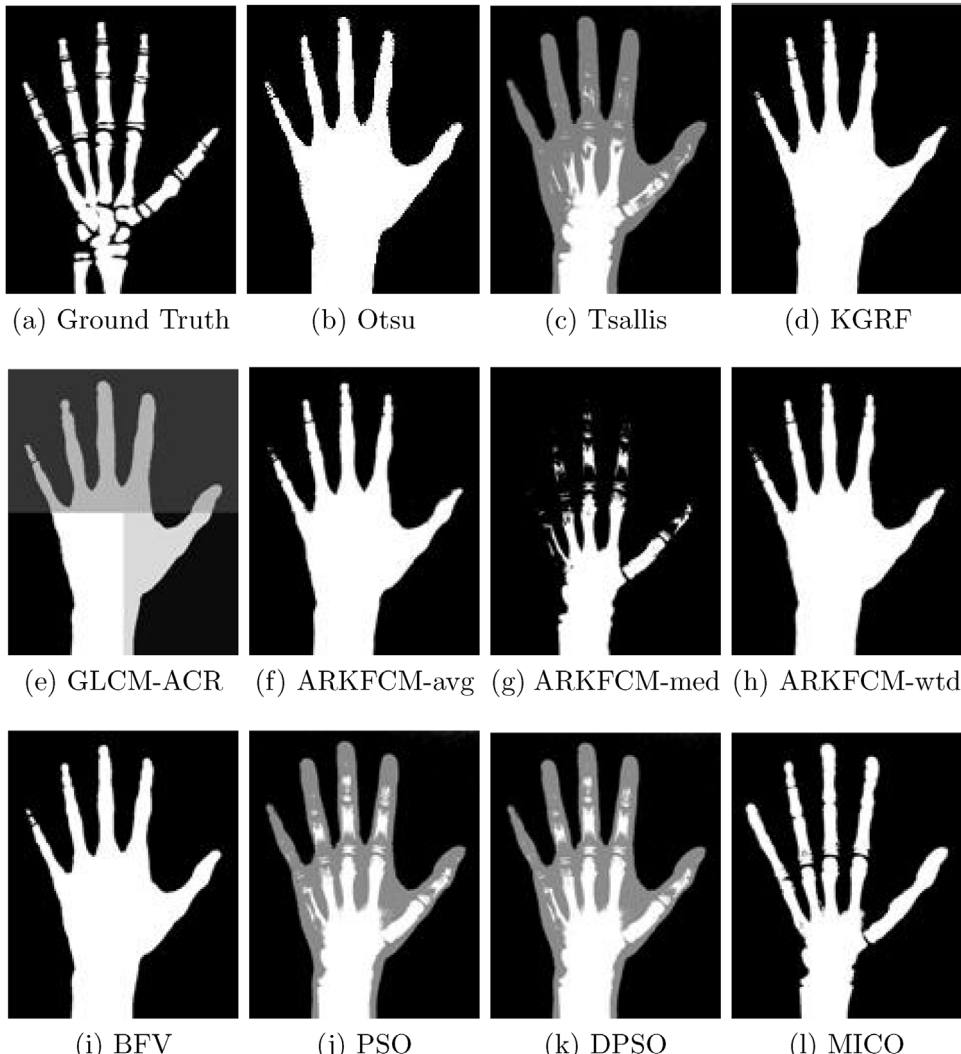


**Fig. 6.** Segmentation results of different algorithms on hand radiograph taken from 10 year old person [5217.jpg].

**Table 8**

Quality metric results for segmentation of hand radiograph taken from 16 year old person [5208.jpg].

Techniques	PSNR	MSE	SSIM	JSI	Dice	ACC	Time(s)
Otsu [11]	47.01	1.30	0.85	0.21	0.28	0.52	5.54
Tsallis [28]	57.52	0.12	0.99	0.47	0.64	0.73	<b>2.84</b>
KGRF [13]	58.85	0.08	0.99	0.65	0.79	0.83	79.99
GLCM-ACR [18]	7.07	12775.13	0.00	0.21	0.00	0.01	16.54
ARKFCM-avg [29]	58.35	0.10	0.99	0.68	0.81	0.84	355.43
ARKFCM-med [29]	58.35	0.09	0.99	0.68	0.81	0.84	351.39
ARKFCM-wtd [29]	58.35	0.10	0.99	0.68	0.81	0.84	356.44
BFV [30]	58.03	0.10	0.99	0.67	0.80	0.83	109.65
PSO [31]	58.82	0.09	0.99	0.65	0.79	0.83	13.76
DPSO [32]	58.82	0.09	0.99	0.65	0.79	0.83	12.70
MICO [33]	<b>62.28</b>	<b>0.04</b>	<b>1.00</b>	<b>0.84</b>	<b>0.91</b>	<b>0.92</b>	109.54

Highlighted value signifies the best result among all algorithms.

PSNR value of KGRF algorithm is highest, with Tsallis, PSO, DPSO and ARKFCM algorithm having closer values. Table 4 shows results obtained from hand radiograph of 8 year old person. We can see that MICO algorithm has highest segmentation accuracy values but Tsallis algorithm takes least time. The time taken by MICO algorithm is almost 10 times than that of Tsallis algorithm. In Tables 5, 6, 7, 8 and 9 we see that MICO algorithm gives the best results for segmentation accuracy and none of the other algorithms have comparable

**Table 9**

Quality metric results for segmentation of hand radiograph taken from 18 year old person [6145.jpg].

Techniques	PSNR	MSE	SSIM	JSI	Dice	ACC	Time(s)
Otsu [11]	58.60	0.09	0.99	0.73	0.84	0.86	4.06
Tsallis [28]	57.77	0.11	0.99	0.70	0.82	0.85	<b>1.46</b>
KGRF [13]	58.45	0.09	0.99	0.72	0.84	0.86	65.35
GLCM-ACR [18]	6.75	13758.6	0.01	0.26	0.01	0.01	16.01
ARKFCM-avg [29]	58.08	0.10	0.99	0.71	0.83	0.86	294.32
ARKFCM-med [29]	58.09	0.10	0.99	0.71	0.83	0.86	295.30
ARKFCM-wtd [29]	58.08	0.10	0.99	0.71	0.83	0.86	293.23
BFV [30]	56.37	0.15	0.98	0.63	0.77	0.81	106.89
PSO [31]	58.57	0.09	0.99	0.73	0.84	0.86	11.08
DPSO [32]	58.60	0.09	0.99	0.73	0.84	0.86	10.76
MICO [33]	<b>61.57</b>	<b>0.05</b>	<b>0.99</b>	<b>0.85</b>	<b>0.92</b>	<b>0.92</b>	69.55

Highlighted value signifies the best result among all algorithms.

values. Also the time taken by Tsallis is least for all the hand radiographs with MICO taking 10 times more time. The time taken by algorithm is varying because the hand radiograph images are of different sizes.

#### 4.2. Qualitative analysis

The qualitative analysis of various evolutionary and non-evolutionary segmentation techniques have been shown in

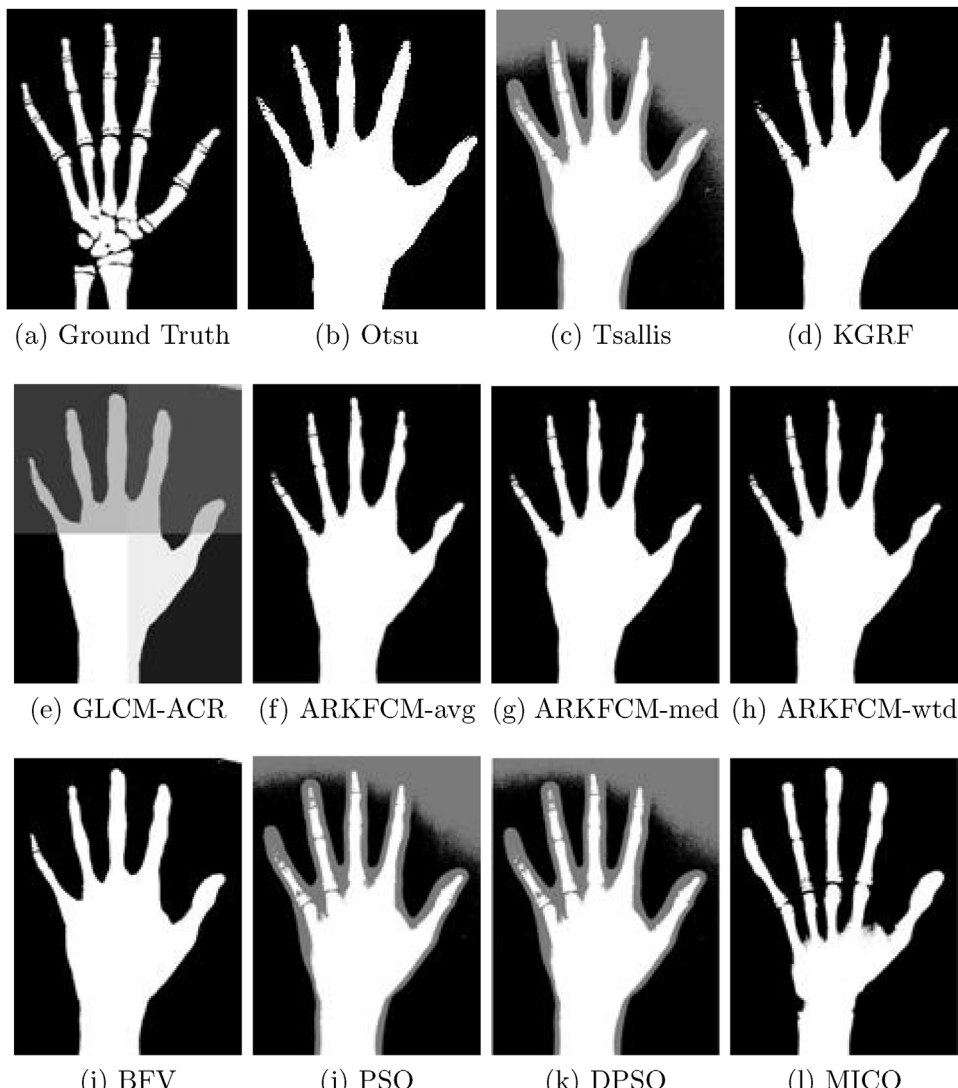


**Fig. 7.** Segmentation results of different algorithms on hand radiograph taken from 12 year old person [5322.jpg].

following figures. Fig. 2 shows results for 2 years old person. Except for MICO algorithm all other segmentation techniques have failed. All bones are not segmented and lost in the procedure. GLCM-ACR algorithm has completely failed by tracking boundary of hand and not the bones.

Fig. 3 shows the segmentation results for 4 years old person. Here also we see that MICO algorithm gives best result as compared to others as they have failed to segment out all the bones.

From the segmentation results shown in Fig. 4 for a hand radiograph of 6 year old person we can say that, apart from MICO algorithm PSO and DPSO algorithms have faired well. But they have failed to segment the bones of pinky/small finger. Rest all results have segmented soft tissue region over the palm of hand.

In Fig. 9 also we can see that PSO and DPSO algorithms have faired well but lost the bones of small and ring fingers. All other algorithms have tracked the boundary on hand rather than segmenting the bones. MICO algorithm has given best rest for this hand radiograph of 8 year old person.

Fig. 6 shows segmentation results evaluated on hand radiograph of 10 year old person. MICO algorithm has performed best among all algorithms. All other algorithms have tracked only the boundary of hand except for PSO and DPSO algorithms which segmented the bones but not all. KGRF and BFV algorithms have tracked the bones of fingers well but rest of the bones are not delineated.

For hand radiograph shown in Fig. 7 the segmentation results show that MICO algorithm has segmented the bones with high accuracy compared to all the other algorithms.

From Fig. 8 we can see that Tsallis algorithm along with PSO and DPSO algorithms have given fair results but still have overlapping regions. KGRF algorithm has performed well but failed to segment bones of pinky finger and of the palm. MICO algorithm has given best results on this hand radiograph of 14 year old person.

From Fig. 9 which shows segmentation results for hand radiograph of 16 year old person we can see that PSO and DPSO techniques have given good results but still have overlapping regions and missed out a bones of last finger. MICO technique has given best result.

In Fig. 10 which shows segmentation results for hand radiograph of 18 year old person we can see that Tsallis, KGRF, ARKFCM, PSO and DPSO segmentation techniques have given good results but still have overlapping regions over the palm region of hand. MICO technique again has given best result among all the algorithms compared.

#### 4.3. Segmentation accuracy

The various quality metrics used namely JSI, Dice and Accuracy give sound information about the segmentation accuracy

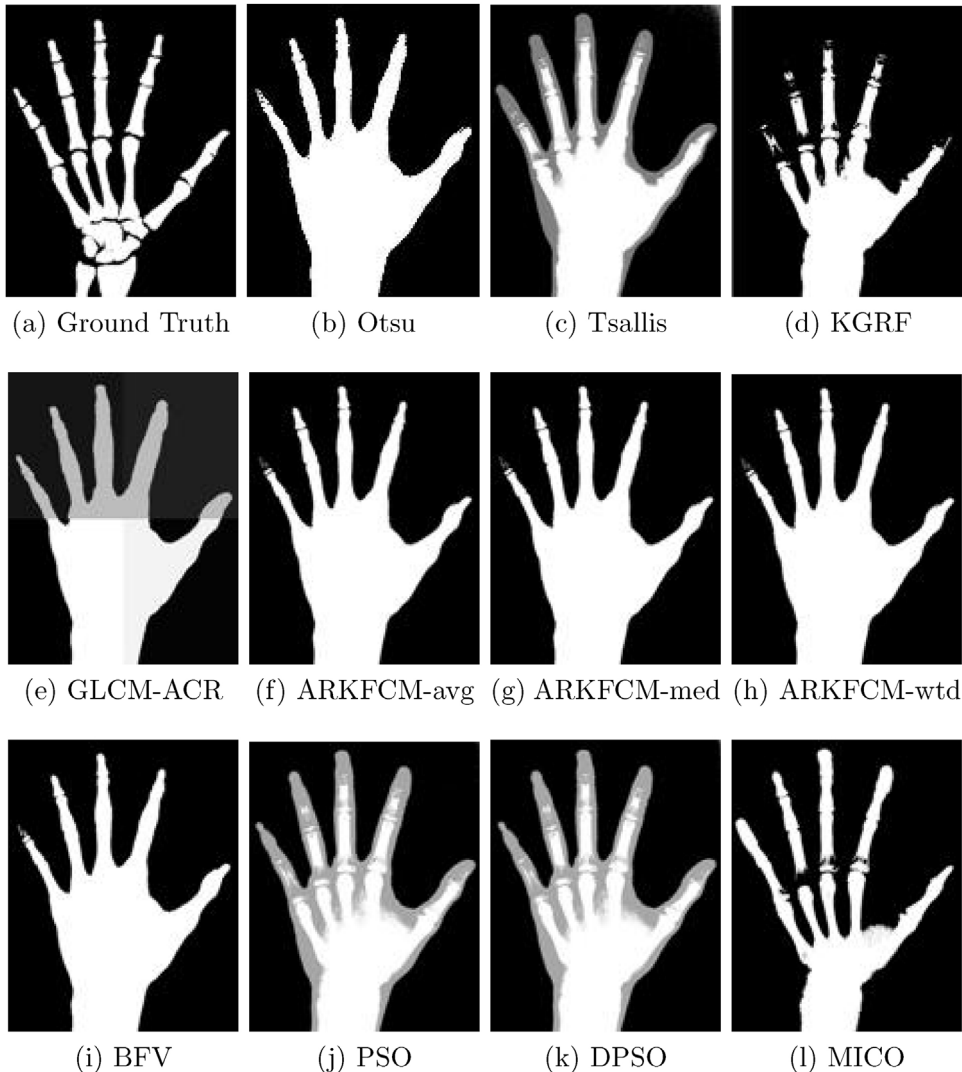


**Fig. 8.** Segmentation results of different algorithms on hand radiograph taken from 14 year old person [5225.jpg].

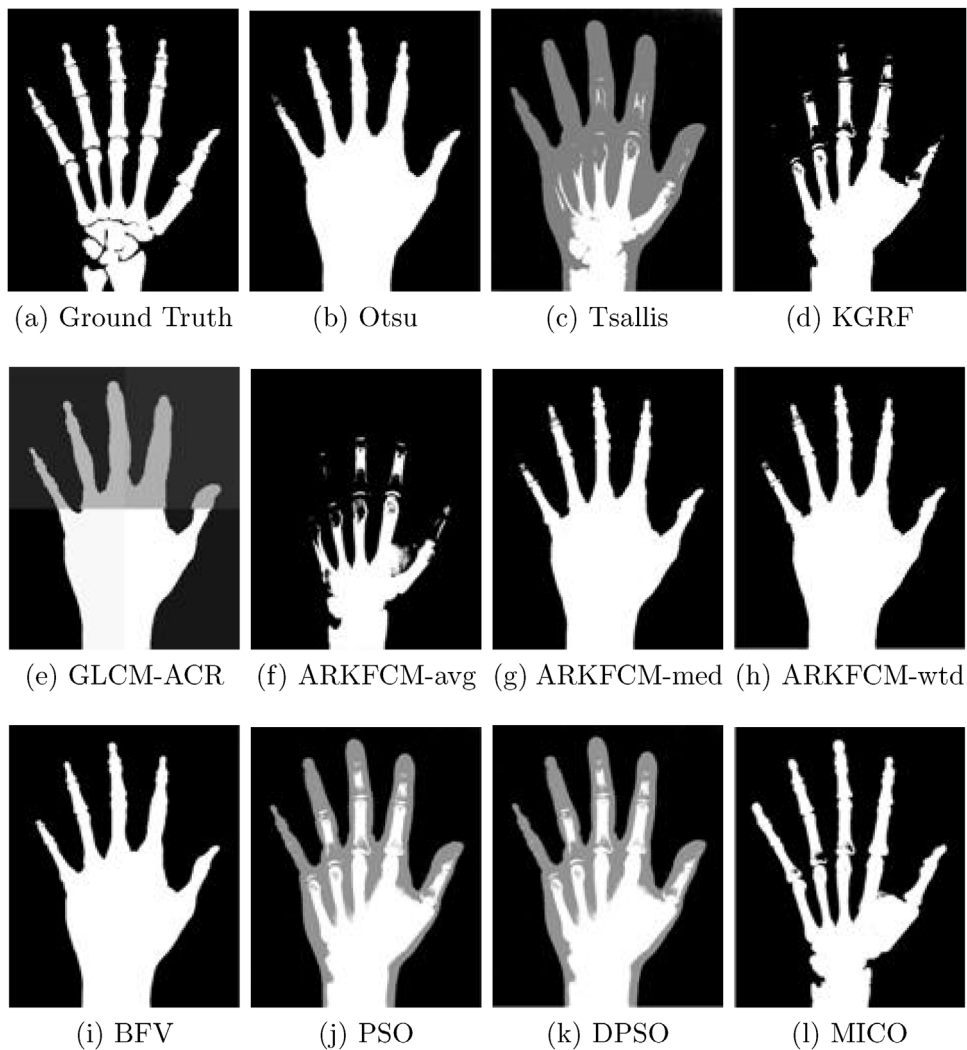


**Fig. 9.** Segmentation results of different algorithms on hand radiograph taken from 16 year old person [5208.jpg].

that has been achieved. The quantitative analysis represented in the tables give clear indication that adaptive crossed reconstruction (ACR) based on GLCM performs very poorly. Segmentation techniques based on Otsu's thresholding and Tsallis entropy also gave unsatisfactory results. KGRF algorithm has performed satisfactorily for hand radiographs above 12 years age, but failed completely for others. ARKFCM technique and BFV technique are two non-evolutionary techniques which have given suitable results compared with evolutionary techniques. Comparing the quality metric results for JSI, Dice and Accuracy from Table 1 to 9, it is noticed that MICO technique performs better than other evolutionary and non-evolutionary techniques. The visual information obtained from Fig. 2 to 10, it is clear that MICO segmentation technique gives results closer to the ground truth as compared to other existing segmentation techniques.

#### 4.4. Computational cost

The time taken by each segmentation technique is mentioned in the last column of each table. From the experimental results obtained we can notice that the computational cost for ARKFCM technique is highest among all the images, and the least being for Otsu's thresholding and Tsallis entropy techniques. The computational cost for MICO technique and techniques like KGRF and BFV are comparable. MICO takes 4–5 times more time

than other evolutionary techniques like PSO and DPSO. Whereas computational cost for ARKFCM is 5–6 times more than that for MICO. The difference in time taken for segmentation is due to different sizes of the images used for experiments.

## 5. Conclusion

This paper highlighted performance evaluation and comparison of different evolutionary and non-evolutionary segmentation techniques on hand radiographs for bone age assessment. The segmentation techniques used for comparison are recent and advanced. From our literature survey in the field of Bone Age Assessment, we found that there was hardly any comparison done between various evolutionary and non-evolutionary segmentation techniques implemented on digital hand radiographs. Also the segmentation techniques implemented on hand radiographs have not been evaluated using standard quality metrics. Computational cost for segmentation was not computed either. The segmentation techniques thus compared in this paper are light on computation cost.

The experimental results revealed that MICO technique provided best segmentation result as compared with other mentioned evolutionary and non-evolutionary segmentation techniques. In spite of being 4–5 times slower than PSO and DPSO methods the quality of results obtained using MICO technique supersedes the other techniques. Computational cost of MICO can be attributed

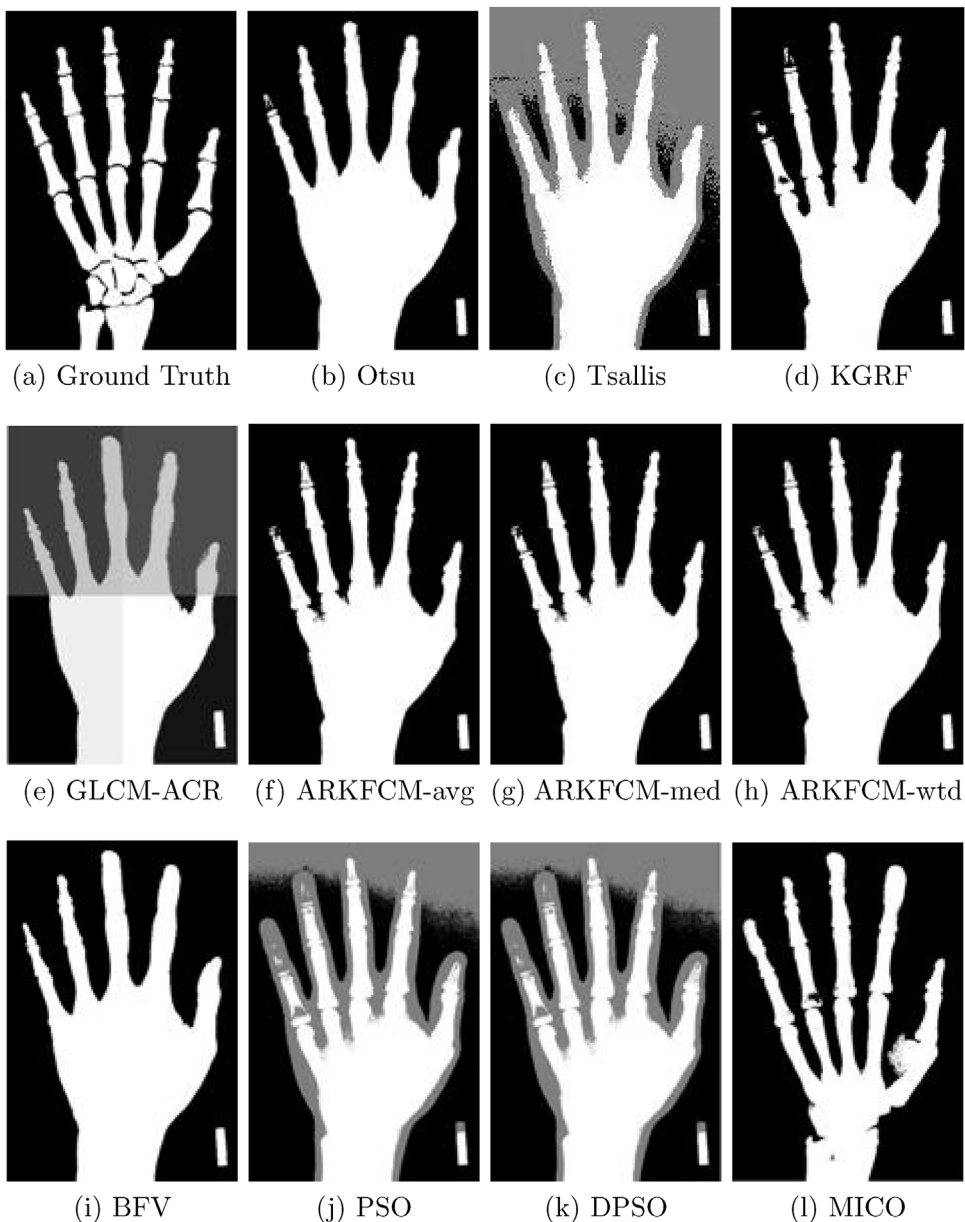


**Fig. 10.** Segmentation results of different algorithms on hand radiograph taken from 18 year old person [6145.jpg].

to the fact that it decomposes the image into two multiplicative components and removes the intensity inhomogeneity.

MICO technique has some overlapping regions in the hand radiographs of ages less than 8 years old which can be improved. The radiation intensity used is weaker for younger children and the X-ray equipment also introduces some noise. However MICO technique has given good results in this situation. It is deemed unethical and also considered harmful to take radiographs of children less than 2 years age so it has not been included.

Further work can be done to reduce the computational cost for MICO technique. Finally from qualitative and quantitative analysis of evolutionary and non-evolutionary techniques we can say that MICO is the best segmentation technique that can be applied on hand radiographs for bone age assessment.

#### Acknowledgements

The authors would like to thank Dr. Kunal Fadte and his team from Goa Medical College, Goa, India, for helping with creation of

ground truth images and validating the segmentation results. The authors would also like to thank anonymous reviewers for their valuable suggestions and comments which helped to improve the quality of the research paper.

#### References

- [1] V. Gilsanz, O. Ratib, *Hand Bone Age: A Digital Atlas of Skeletal Maturity*, Springer Science & Business Media, 2005.
- [2] W.W. Greulich, S.I. Pyle, Radiographic atlas of skeletal development of the hand and wrist, *Am. J. Med. Sci.* 238 (1959) 393.
- [3] J.M. Tanner, *Growth at Adolescence*, 1962.
- [4] J. Tanner, M. Healy, H. Goldstein, N. Cameron, *Assessment of Skeletal Maturity and Prediction of Adult Height: TW3 Method*, 2001.
- [5] E. Pietka, A. Gertych, S. Pospiech, F. Cao, H. Huang, V. Gilsanz, Computer-assisted bone age assessment: image preprocessing and epiphyseal/metaphyseal ROI extraction, *IEEE Trans. Med. Imaging* 20 (2001) 715–729.
- [6] J. Zhang, H. Huang, Automatic background recognition and removal (ABRR) in computed radiography images, *IEEE Trans. Med. Imaging* 16 (1997) 762–771.

- [7] E. Pietka, M.F. McNitt-Gray, M. Kuo, H. Huang, Computer-assisted phalangeal analysis in skeletal age assessment, *IEEE Trans. Med. Imaging* 10 (1991) 616–620.
- [8] E. Pietka, L. Kaabi, M. Kuo, H. Huang, Feature extraction in carpal-bone analysis, *IEEE Trans. Med. Imaging* 12 (1993) 44–49.
- [9] B. Sharif, S. Zaroug, E. Chester, J. Owen, E. Lee, Bone edge detection in hand radiographic images, in: Proceedings of the 16th Annual International Conference of the IEEE Engineering in Medicine and Biology Society, Engineering Advances: New Opportunities for Biomedical Engineers, IEEE, 1994, pp. 514–515.
- [10] D. Giordano, R. Leonardi, F. Maiorana, G. Scarciofalo, C. Spampinato, Epiphysis and metaphysis extraction and classification by adaptive thresholding and DoG filtering for automated skeletal bone age analysis, in: 29th Annual International Conference of the IEEE Engineering in Medicine and Biology Society, EMBS 2007, 2007, pp. 6551–6556.
- [11] N. Otsu, A threshold selection method from gray-level histograms, *Automatica* 11 (1975) 23–27.
- [12] M. Kashif, S. Jonas, D. Haak, T.M. Deserno, Bone age assessment meets SIFT, in: SPIE Medical Imaging, International Society for Optics and Photonics, 2015, p. 941439.
- [13] T.N. Pappas, An adaptive clustering algorithm for image segmentation, *IEEE Trans. Signal Process.* 40 (1992) 901–914.
- [14] E. Pietka, S. Pospiech-Kurkowska, A. Gertych, F. Cao, Integration of computer assisted bone age assessment with clinical pacs, *Comput. Med. Imaging Graph.* 27 (2003) 217–228.
- [15] A. Zhang, A. Gertych, B.J. Liu, Automatic bone age assessment for young children from newborn to 7-year-old using carpal bones, *Comput. Med. Imaging Graph.* 31 (2007) 299–310.
- [16] A. Tristan-Vega, J.I. Arribas, A radius and ulna TW3 bone age assessment system, *IEEE Trans. Biomed. Eng.* 55 (2008) 1463–1476.
- [17] D. Giordano, C. Spampinato, G. Scarciofalo, R. Leonardi, An automatic system for skeletal bone age measurement by robust processing of carpal and epiphyseal/metaphysial bones, *IEEE Trans. Instrum. Meas.* 59 (2010) 2539–2553.
- [18] H.Y. Chai, L.K. Wee, T.T. Swee, S. Hussain, GLCM based adaptive crossed reconstructed (ACR) k-mean clustering hand bone segmentation, in: Proceeding of 10th WSEAS International Conference on Electronics, Hardware, Wireless and Optical Communications, and 10th WSEAS International Conference on Signal Processing, Robotics and Automation, and 3rd WSEAS International Conference on Nanotechnology, and 2nd WSEAS International Conference on Plasma-Fusion-Nuclear Physics, 2011, pp. 192–197.
- [19] R.C. Gonzalez, R.E. Woods, S.L. Eddins, Digital Image Processing Using MATLAB, Pearson Education India, 2004.
- [20] G. Manos, A. Cairns, I. Rickets, D. Sinclair, Segmenting radiographs of the hand and wrist, *Comput. Methods Programs Biomed.* 43 (1994) 227–237.
- [21] Y.C. Hum, Segmentation of Hand Bone for Bone Age Assessment, Springer, 2013.
- [22] M. Niemeijer, B. van Ginneken, C.A. Maas, F.J. Beek, M.A. Viergever, Assessing the skeletal age from a hand radiograph: automating the tanner-whitehouse method, in: Medical Imaging 2003, International Society for Optics and Photonics, 2003, pp. 1197–1205.
- [23] D. Luis-Garcia, M. Martin-Fernández, J.I. Arribas, C. Alberola-López, et al., A fully automatic algorithm for contour detection of bones in hand radiographs using active contours, in: 2003 International Conference on Image Processing, ICIP 2003. Proceedings, vol. 3, IEEE, 2003, p. III-421.
- [24] H.H. Thodberg, S. Kreiborg, A. Juul, K.D. Pedersen, The boneXpert method for automated determination of skeletal maturity, *IEEE Trans. Med. Imaging* 28 (2009) 52–66.
- [25] C.-C. Han, C.-H. Lee, W.-L. Peng, Hand radiograph image segmentation using a coarse-to-fine strategy, *Pattern Recogn.* 40 (2007) 2994–3004.
- [26] J. Liu, J. Qi, Z. Liu, Q. Ning, X. Luo, Automatic bone age assessment based on intelligent algorithms and comparison with TW3 method, *Comput. Med. Imaging Graph.* 32 (2008) 678–684.
- [27] P. Thangam, K. Thanushkodi, T. Mahendiran, PSO for graph-based segmentation of wrist bones in bone age assessment, *Int. J. Comput. Commun. Control* 8 (2012) 153–160.
- [28] M.P. de Albuquerque, I. Esquef, A.G. Mello, Image thresholding using Tsallis entropy, *Pattern Recogn. Lett.* 25 (2004) 1059–1065.
- [29] A. Elazab, C. Wang, F. Jia, J. Wu, G. Li, Q. Hu, Segmentation of brain tissues from magnetic resonance images using adaptively regularized kernel-based fuzzy-means clustering, in: Computational and Mathematical Methods in Medicine 2015, 2015.
- [30] M. Gong, D. Tian, L. Su, L. Jiao, An efficient bi-convex fuzzy variational image segmentation method, *Inform. Sci.* 293 (2015) 351–369.
- [31] R.C. Eberhart, J. Kennedy, A new optimizer using particle swarm theory, in: Proceedings of the Sixth International Symposium on Micro Machine and Human Science, vol. 1, New York, NY, 1995, pp. 39–43.
- [32] J. Tillett, T. Rao, F. Sahin, R. Rao, Darwinian Particle Swarm Optimization, 2005.
- [33] C. Li, J.C. Gore, C. Davatzikos, Multiplicative intrinsic component optimization (MICO) for MRI bias field estimation and tissue segmentation, *Magn. Reson. Imaging* 32 (2014) 913–923.
- [34] R.M. Haralick, Statistical and structural approaches to texture, *Proc. IEEE* 67 (1979) 786–804.
- [35] J.C. Bezdek, Pattern Recognition with Fuzzy Objective Function Algorithms, Springer Science & Business Media, 2013.
- [36] T.F. Chan, L. Vese, et al., Active contours without edges, *IEEE Trans. Image Process.* 10 (2001) 266–277.
- [37] P. Ghamisi, M.S. Couceiro, N.M.F. Ferreira, L. Kumar, Use of Darwinian particle swarm optimization technique for the segmentation of remote sensing images, in: IEEE International Geoscience and Remote Sensing Symposium (IGARSS), IEEE, 2012, pp. 4295–4298.
- [38] P. Perona, J. Malik, Scale-space and edge detection using anisotropic diffusion, *IEEE Trans. Pattern Anal. Mach. Intell.* 12 (1990) 629–639.
- [39] D. Gupta, R. Anand, B. Tyagi, A hybrid segmentation method based on Gaussian kernel fuzzy clustering and region based active contour model for ultrasound medical images, *Biomed. Signal Process. Control* 16 (2015) 98–112.